HiSST: 2nd International Conference on
High-Speed Vehicle Science & Technology
11–15 September 2022, Bruges, Belgium

Performance of vehicle-integrated scramjet inlets on a wing-cone accelerating vehicle

Damian Curran[1], *Vincent Wheatley*[2], *Rowan Gollan*[3], *Michael Smart*[4]

Keywords: *scramjet, inlet, hypersonic, cfd*

1. Introduction

Scramjet engines can revolutionise high speed flight due to their high specific impulse, with applications ranging from access-to-space and transport at cruise conditions. However, a scramjet must be designed in concert with the vehicle for a multitude of reasons, as discussed by Heiser and Pratt [1]. One of the key drivers of this is the superlinear scaling of the capture area of the engine with increasing Mach number [2], [3]. This physical requirement leads to airframe-integrated engines, where the design of the inlet is entwined with the design of the vehicle. This has been a recognised design approach for scramjets since the 1970s, in foundational works such as [4], [5], [6], and [7].

A few approaches for integrated inlet design have emerged. Increasing in complexity, these range from 2D planar and axisymmetric, to sidewall compression and other 3D inward-turning inlets. 2D and sidewall compression inlets are plagued by a range of issues, such as corner effects in their rectangular combustors, and separation due to cowl closure shocks. A discussion on Korkegi's [8] work on boundary layer separation in [9] details how a swept interaction like those in 3D turning inlets is less likely to cause unstart than a planar 2D shock (examples of which are shown in [10] and [11]). Inward-turning, axisymmetric inlets are poor from a vehicle packing perspective, however, their circular combustors are attractive to an engine designer from the perspective of lowest-wetted-area and structural strength. An elliptical combustor edges in front of a circular one when considering wetted area and penetration/mixing. So, a method of capturing vehicle forebody airflow, compressing it efficiently to desired combustor pressures and temperatures, and matching the combustor entrance shape is required. All this is preferable as a fixed geometry system. This motivates the shape-transition inlet designs. There are currently few proven design techniques to build a vehicle-integrated compression system.

The search started in the 1960s when researchers began streamline tracing inlets [12] - modifying one capture shape into another at the combustor. These researchers were limited by the computational power at the time. Smart [13] revived this process with a Rectangular to Elliptical Shape-Transition (REST) technique, where an inlet was traced forwards from a modular capture shape, and backwards from a combustor shape to generate an inlet which could be stacked underneath a vehicle. This inlet tracing technique is inviscid, with a "simple" boundary layer correction applied to relax the physical compression inline with boundary layer growth.

Other design techniques have been attempted over the years - an early attempt at streamline tracing [14], another style of parent flowfield and blending [15], [16], variable geometry ramp inlets [14], contouring through streamline "cutting" [17], and streamline traced inlets for waverider class vehicles [17].

The REST inlet class have been well studied - they operate well from Mach 4 [18] to Mach 12 [19], [20], as well as at off-design conditions [21]. Originally the inlet class was designed for a planar forebody,

[1] *Centre for Hypersonics, UQ*
[2] *Centre for Hypersonics, UQ*
[3] *Centre for Hypersonics, UQ*
[4] *Hypersonix Launch Systems*

but Gollan and Smart [22] extended the design methodology to fit on conical vehicles. All these factors make it attractive as the basis of the inlet design for an accelerating scramjet engine.

In their work, Gollan and Smart [22] designed the inlet on the centre-line of the vehicle, although it was for use at angle of attack and in a modular manner. There was an assumption that the inlet would be sufficiently robust to operate off-design in the described way. This work tests the assumption that a boundary-layer-corrected, inviscid inlet design on a vehicle centreline is applicable for use away from this design point. It does this by investigating an inlet designed in a similar manner, at angle of attack and as four modules taking up 180 degrees of the vehicle frontage.

The context for the inlet design is an extensive study at the Centre for Hypersonics in the University of Queensland, which is to develop a scramjet engine to accelerate from Mach 5 to Mach 10. An accelerating scramjet engine is an attractive option for the second stage of a three stage launch system [23]. The scramjet engine can decrease the cost of access to space through its increased payload mass fraction, higher specific impulse through its operating regime, and inherent re-usability [24].

This paper discusses the robustness of the design technique, and numerically investigates the performance of the CREST (CRescent to Elliptical Shape Transitioning) inlet as designed by Gollan and Smart. This inlet is to be used on SPARTAN, the second stage of the launch system. The paper briefly discusses the design process, before assessing performance and characterising the flowfield at discrete Mach numbers between Mach 5 and 10, and angles of attack of 0, 2, and 4. No such inlet exists, that can provide adequate compression over such a large speed range (especially without moving parts to modify the compression).

Fig 1. Depiction of scramjet 2nd stage releasing the 3rd stage rocket [24].

2. Inlet Design Methodology

This section discusses some design choices relevant to an inlet for an access-to-space trajectory. A target pressure of 50 kPa at the design condition was chosen (Mach 10), leading to higher pressures at the throat at lower speeds due to the constant dynamic pressure trajectory.

The first thing to consider is the requirements of the mission. In this case, this mission is to accelerate a payload from Mach 5 to Mach 10 at 50kPa dynamic pressure. An accelerator vehicle needs a good

thrust margin [25] at its peak speed to ensure a short duration flight. In this case, an access-to-space scramjet vehicle requires hydrogen fuel due to its specific energy density. However, hydrogen also has a large physical density, and a large vehicle is required to store both the fuel, and the third stage rocket. Although a planar vehicle has a high performing forebody - a wedge works well with angle of attack and regarding inlet stacking - it lacks the storage potential of a conical vehicle.

Another major benefit of the conical forebody is the reduced boundary layer. This increases the quality of captured air at the throat, by lowering spillage and capturing more air than the same inlet on a planar - or other - forebody. More captured air equates to higher thrust, through a greater equivalence ratio and the presence of more mass through the engine alone.

On balance, the conical vehicle was chosen for this application as discussed by [26]. The choice of cone forebody sets some constraints on the inlet design.

After deciding on the vehicle shape and the inlet design methodology (choosing Smart and Gollan's streamline tracing approach), the next choice is the number of inlets. The extremes are a single engine module, and 360 degree coverage of the vehicle forebody through multiple modules. A scramjet designer wishes to make full use of air processed by the forebody. For a vehicle flying at angle of attack (as this one does), only the underside of the vehicle compresses the air.

So the two questions for design are: how much of this air is useful, and how many intakes are required? Neither have a definite answer. Gollan and Smart decided to make use of 180 degrees of the vehicle, to capture all sensibly processed air. More than 180 degrees, and the inlets begin to ingest air that, at an angle of attack, is becoming far from ideal. Less than 180 degrees results in missing useful air.

The question of intake number is another of trade-offs. Fewer inlets translates to reduced wetted area; less viscous drag, but then leads to difficulty in penetrating the core flow. Conversely, more inlets leads to more sensible combustor geometries at the expense of more stacking arrangements and increased wetted area. The final consideration is the behaviour of the streamline tracing through the parent flowfield. Choosing three engine modules moved the capture shape away from the heritage REST-class aspect ratio, and led to throat shapes sticking into the freestream. Drag on these dropped surfaces should be avoided; this is covered further in [22]. The authors determined four inlets to be an appropriate balance between these competing factors.

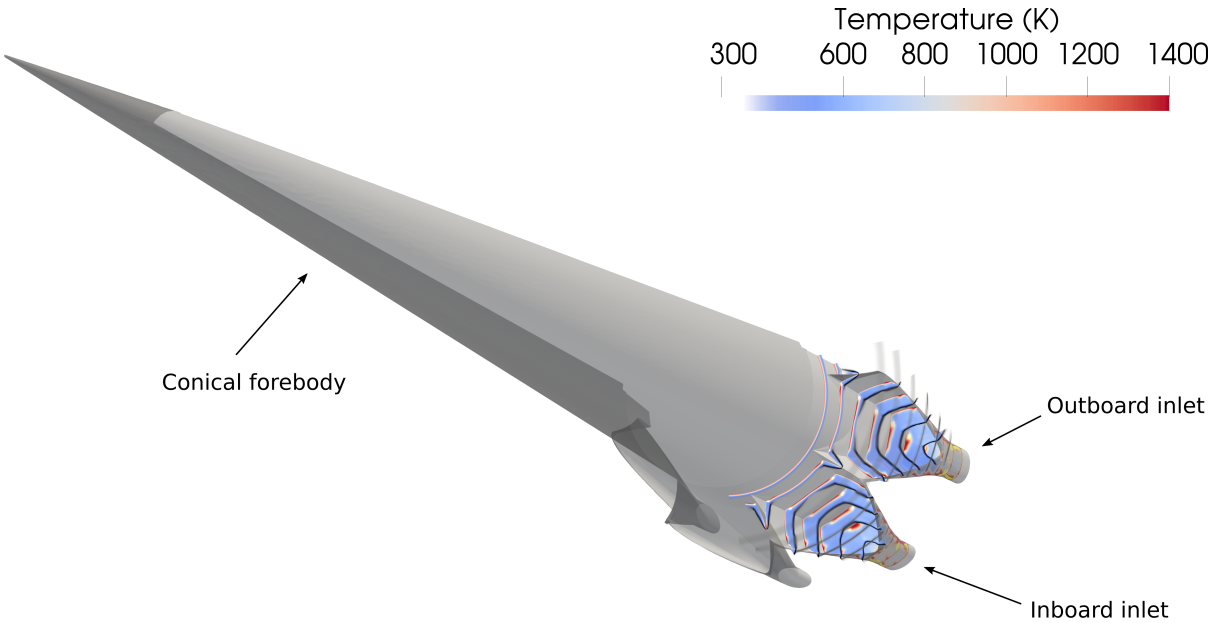

Fig 2. The placement of the inlets on the conical forebody, with shock structure and temperature contours apparent through the inlets.

There are still some considerations for the inlet design. At this point, it is prudent to understand the conical forebody implementation of Smart's [13] work - by Gollan and Smart [22]. That work discusses in great detail the methodology behind the inlet.

The inlet should be designed for Mach 10, where the shocks are closest to the vehicle. By doing this, the forebody shocks will never impinge inside the inlet. The start of the trajectory, Mach 5, bounds the design with another constraint; that of inlet starting.

The issue of an inlet self-starting has remained throughout the history of scramjets - the ability for the flow to be supersonic throughout the flowpath without the use of doors or other complicated and weighty features. The Kantrowitz [27] limit is a well-known experimental correlation for the self-starting of 2D inlets based on their internal contraction. (Internal contraction is the ratio of area reduction from the first completely enclosed part of the inlet to the throat.) Variable geometry inlets will provide a started inlet, at a large weight and engineering cost. This can be avoided by using a fixed-geometry inlet which is self-starting.

Two-dimensional inlets have a severe restriction on the amount of internal contraction; Smart [9] has plotted a 3D limit, which is more relaxed due to 3D relieving effects. A benefit of the shape-transition inlets is their naturally mixed compression. The balance is shifted to greater external compression by cutting the cowl further along the inlet, to spill more flow and have a lower Mach number at the cowl.

The lowest cowl Mach number, at Mach 5, sets the internal area contraction. Once this condition is satisfied, the inlet design can proceed and the inlets bounds are safe.

The inlet was designed along the centreline of the vehicle. The choice of four inlets means that none will be sitting on the centreline, as shown in Figure 4. This makes the design more conservative, as it provides greater depth from the shock at the design condition, increasing the angle of attack operating envelope of the system.

A final comment on the inlet design is that with angle of attack operation the inlets will see different inflow; as the flow sweeps around the vehicle the shock and compression field will change. A modular approach may not be the optimum, but does provide robustness. The effect of angle of attack operation between the two inlets is discussed throughout the work.

To summarise, the inlet design was fed by several choices: a conical forebody, four modular inlets, meeting a minimum combustor pressure at Mach 10, α =2, and having an internal contraction below the 3D starting limit at Mach 5.

3. Methodology

To investigate the flowfields generated by the inlets to assess their performance, they were simulated using the program US3D [28], to solve the compressible Reynold's Averaged Navier-Stokes equations. This has been used in the past to simulate scramjet inlet flowfields, successfully comparing against experimental data for similar inlet shapes [29], [30], [31]. A hybrid second-order Steger-Warming method [32] is used to calculate the inviscid fluxes, while the viscous fluxes are calculated with a second order central difference MUSCL scheme, on the conserved variables and turbulent viscosity. The solution was integrated in time with an implicit time-marching scheme, accelerated by data parallel line relaxation [33]. Turbulent Prandtl and Schmidt numbers were set to 0.9 and 0.7 respectively. Blottner curve fits are used to calculate species-specific viscosity. Thermal equilibrium was assumed. Further information on the solver can be found in [28]. The flowfield was run laminar until the start of the inlet where physical trips would be placed to transition the flow from laminar to turbulent. From here turbulence was allowed to develop in the rest of the flowfield. The Spalart-Allmaras turbulence model [34] with Catris-Aupiox correction [35] was used for the turbulent parts of the solution.

Two inlets were simulated for computational efficiency - only effect of angle of attack was investigated. Four successively finer structured grids were generated with Gridpro v6.5SP1 [36]. The number of cells

for each grid from coarse to fine were: 20M, 34M, 48M and 78M. Figure 3 shows the throat property convergence behaviour was oscillatory, [37]. However, due to the discrepancy below 1% of the fine grid solution for all solutions, the simulations were considered converged.

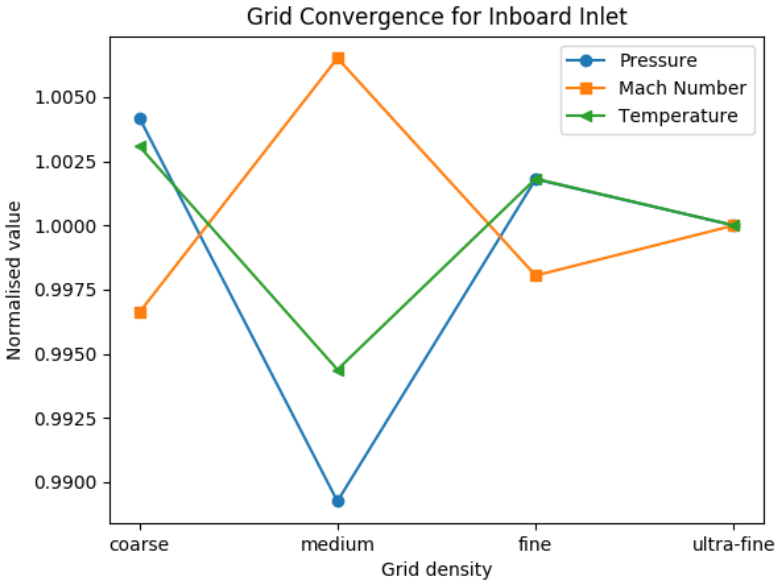

Fig 3. Oscillatory convergence of the solution with increasing grid density.

4. Inlet Flowfield

Before exploring inlet performance, it is instructive for the reader to understand the flowfield produced by each inlet. As well, understanding the difference between each inlet's flowfield is important for the design of the injection scheme; if there are major differences in flowfields, the engines may require separate combustor designs. The general flowfield development through each inlet is discussed using the Mach 10 α = 2 flowfield (the nominal design condition).

Figure 4 depicts the inlet flowfield development using temperature contours, the Q-criterion (which measures where rotation dominates over irrotational strains), and shock structure, with slices perpendicular to each inlet's axis. At this (on-design) flight condition the forebody shock sits just below the cowl of the inboard inlet. There is a greater distance between the forebody shock and the outboard inlet cowl closure. Clear asymmetry in each inlet develops due to the lateral (in the slice plane of reference) movement of the air processed by the forebody shock. Lateral flow is zero at the midplane and increases away from it, thus more severely affecting the flow in the outboard inlets, which consequently develop greater asymmetry.

Both inlets exhibit flow features inherent to REST-class inlets. The flowfield of this class of inlet has been well characterised and discussed by Barth [38]. This work does not intend to replicate his analysis of the inlet flow features, but rather draws attention to how a practical configuration affects them.

A useful metric to show some of the inlet flow features is the Q-Criterion; which is is used to show connected regions of high vorticity. Thus the vortices which stretch downstream can be visualised. As the walls penetrate from the vehicle surface a corner vortex is generated, as labelled in Figure 4. On the outer side of both inlets the vortex is stronger through the lateral velocity interaction with this protruding wall. Thus uneven growth affects the development of the boundary layer on the bodyside on the inlets. The thicker, central part of the bodyside boundary layer - inherent to airframe integrated

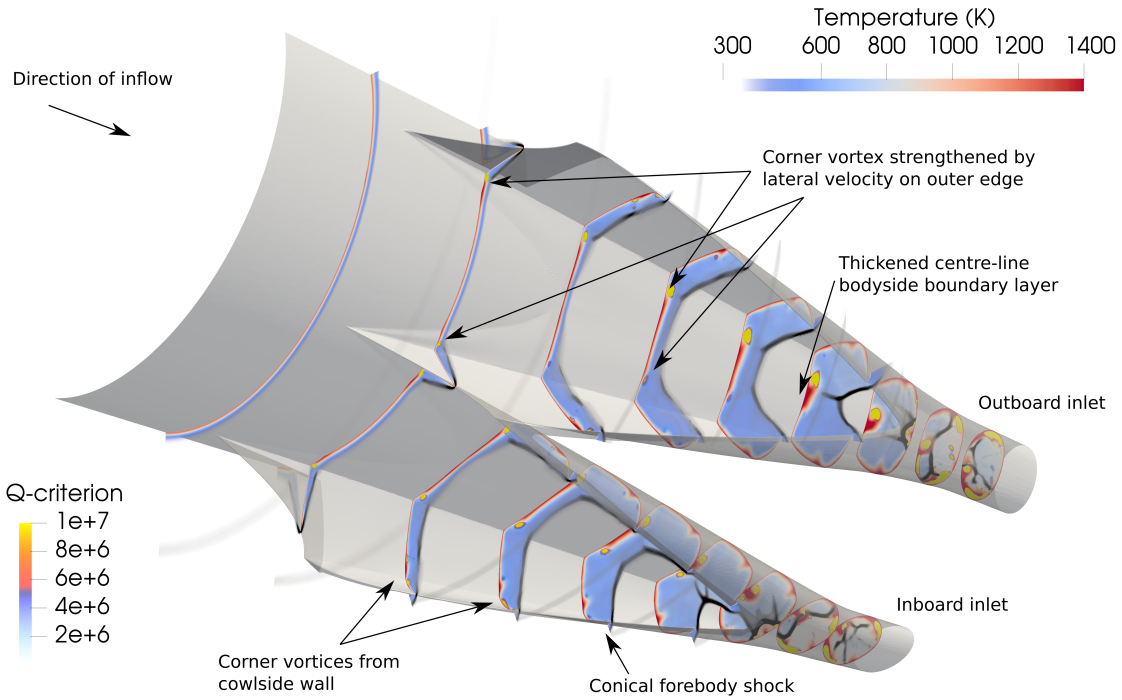

Fig 4. Slices along the inlets showing temperature contours, the Q-criterion (a measure of vorticity), and shock structure as the captured air is compressed. The conical shock passes below the cowl closure of the inlets.

scramjet engines, and shown through the temperature contours - is shifted towards the centreline of the vehicle.

Similarly when the cowl wall penetrates off the sidewall (labelled in Figure 4) the outer edge of each inlet houses a stronger vortex. When the uneven shocks from the sidewalls meet near the cowl closure (and associated shock), further asymmetric vortexes are generated. These sweep around the perimeter of the inlet towards the bodyside and thicken the already-swollen boundary layer (from the cowl-sidewall vortices). The different strengths lead to differently-shaped boundary layers which is more apparent in the throat flowfields (Figure 7). Temperature contours highlight the boundary layer growth and compression through the inlet. Typically the boundary layer is highest in temperature, and the core flow slightly lower. Both inlets have similar temperatures through the flowfield development, and indeed similar flowfield structures. Although there are minor differences in inlet behaviour, the inlets do a superb job of supplying similar flowfields to their respective combustors. A fuel scheme may not even have to differ between inboard and outboard engines.

In the past, the REST-class scramjets are typically analysed using the centre plane of the engines, (this is the symmetry plane for all other REST-class inlets due to their orientation on planar vehicle forebodies). Although these CREST inlets deviate from a symmetric flowfield, it is still instructive to view the symmetry plane shock structures, shown in Figure 6 for both inlets. The red line in the figure shows the boundary layer growth, and the black contour shows shock structure. The extent of the boundary layer is taken as the point of 99.5% of the freestream enthalpy. The boundary layer grows thickly on the bodyside, before turning back towards the body on interaction with the cowl closure shock. The shocks wrapping around the engine appear at different axial locations, although this is a factor of the different asymmetric features of the inlets than alternate behaviour of the inlets. Boundary layer growth from such a long forebody is restricted by the nature of growth on a conical forebody, and does not block too much of the cross section. This centreline behaviour is similar to all REST-class inlets and indicates fuelling strategies of those engines are applicable for the CREST.

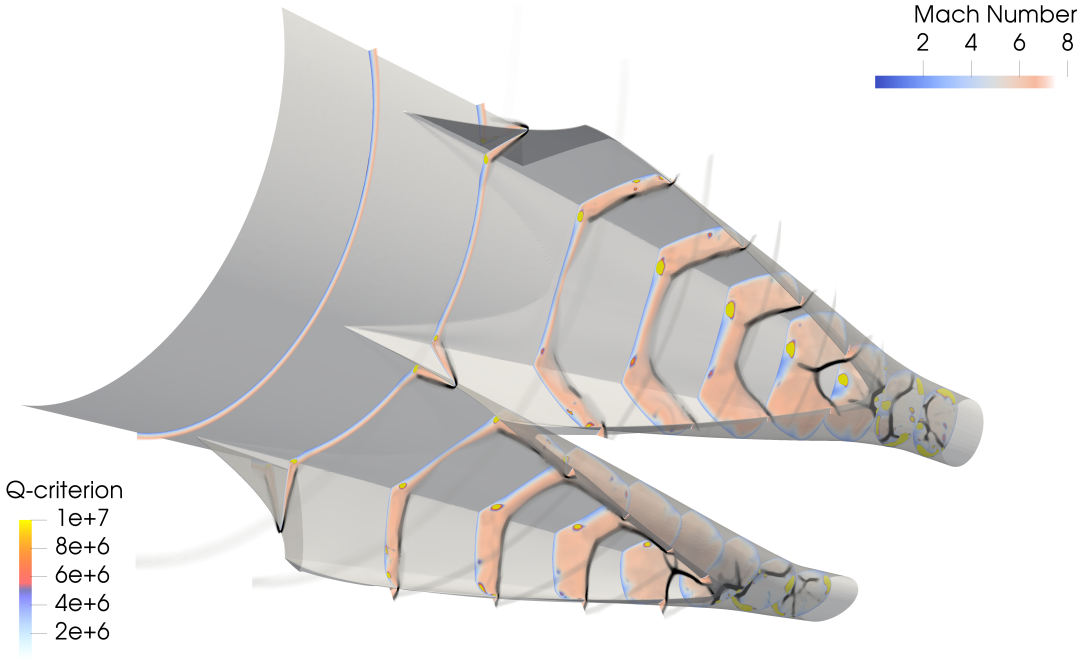

Fig 5. Slices along the inlets showing temperature contours, the Q-criterion (a measure of vorticity), and shock structure as the captured air is compressed. The conical shock passes below the cowl closure of the inlets.

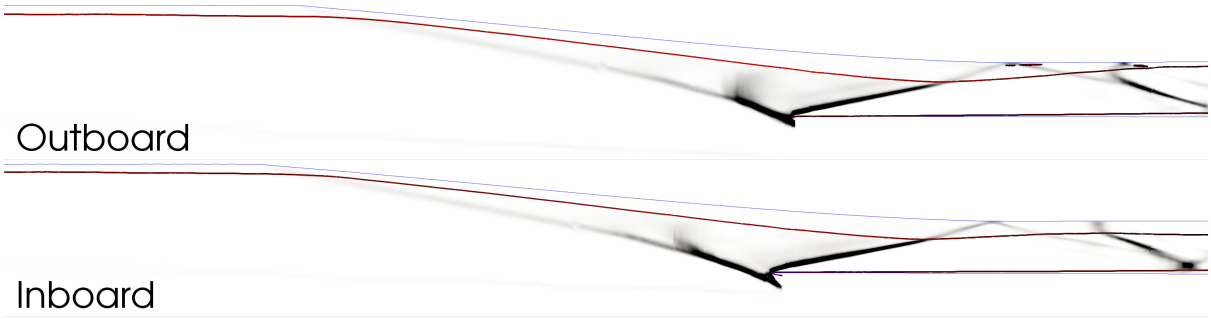

Fig 6. Slices showing shock structure (greyscale contours) and boundary layer growth (red) along the centreplane of both inlets.

Figure 7 shows the throat contours of temperature, with a black line denoting the edge of the boundary layer. The outboard inlet shows greater asymmetry than the inboard. The outer vortex of the bodyside boundary layer is stronger than the one on the inner edge, which curls more of the core flow under the centreline thickening boundary layer. Due to the extra compression on the outer side of the inlet, the bodyside boundary layer thickening is pushed further towards the inside of the inlet. This region is generally targeted by injectors straddling the centreline of the inlet; these injectors will have to shift. The inner edge of both inlets looks remarkably similar, with merging of the sidewall and bodyside swollen boundary layers. On the outer edge there is no merging, as the large bodyside vortex has entrained core flow close to the wall. Also on the outer sidewall is a somewhat more elongated, but cooler section of thick boundary layer (compared to the inner sidewall). None of these asymmetries pose difficult fuelling challenges compared to a completely symmetric inlet; there is already greater asymmetry across the horizontal plane due to the different geometries of the body and cowlsides.

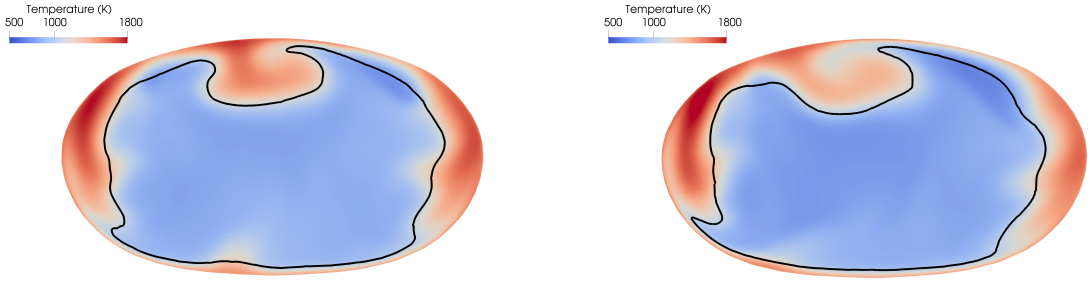

(a) Inboard inlet **(b)** Outboard inlet

Fig 7. Throat contours of temperature of the inboard and outboard inlets. The boundary layer contour is shown with the black line. The ride hand side of each plot is the outer edge of the inlet.

5. Inlet Performance

For the accelerator engine designer, the crucial outputs from the inlet sweep of simulations are the stream-thrust averaged throat conditions. These govern how well the combustor will operate. Although averaged conditions do not capture the three-dimensional effects of the CREST inlets, it is important to know whether the inlet can provide adequate conditions to the combustor throughout the trajectory. Gollan and Smart designed the inlet for the target condition of Mach 10 α = 2 to have an averaged 50 kPa throat condition, often cited for good scramjet performance. Away from this design speed, the inlet's performance will drift. This section looks at the throat conditions across the trajectory to understand whether the combustor will be able to operate. Subsequently, several inlet performance metrics are examined to determine inlet behaviour across the trajectory. All values are stream-thrust averaged.

The most valuable flow properties to explore are pressure, temperature, and Mach number. Figure 10 shows the inboard and outboard throat pressure values. For the inboard inlet at Mach 10 α = 2 has a pressure of 46 kPa, below that of the design pressure. The outboard inlet is lower again, below 40 kPa. As the inlets move away from the centreline of the cone, they capture less mass than the ideal inlet. The reduction of pressure can be thought of in terms of reduced mass capture from the ideal inlet. There is nothing to suggest that pressures below 50 kPa will reduce the performance of the engine, and with the temperatures at Mach 10 (Figure 9), healthy combustion is expected. However, deviating towards a lower angle of attack drops the pressure considerably.

At the opposite end of the trajectory the pressure is higher for both inlets, with more mass capture. On the trajectory (of α = 2) the inboard inlet provides 70 kPa to the combustor, and the outboard, 63 kPa. These values are higher than the target pressure, although not structurally unmanageable. The extra viscous losses are compensated for by the high thrust to drag ratios at low Mach numbers. At Mach 10 the thrust margins are thinner than at the start of the trajectory, and it is crucial that the inlet's performance is targeted towards this point. The CREST inlet (designed by Gollan and Smart) is able to operate over the entire proposed trajectory, which is novel.

The inboard and outboard throat temperatures and Mach numbers are much closer together for the whole test matrix. Figure 8a shows the Mach number throat values, and Figure 9 shows the corresponding temperature. Temperature varies from 630 to 950K on α = 2 trajectory. At Mach 5, even with localised high temperature regions from shock impingements, an ignition system is likely to be required. Through the rest of the trajectory, the inlet delivers reasonable temperatures to the combustor. At Mach 10, the temperature is low enough for the combustion system to avoid dissociating the flow and consequently reducing performance.

Figure 11 shows the pressure recovery both inboard and outboard inlets. Pressure recovery is a measure

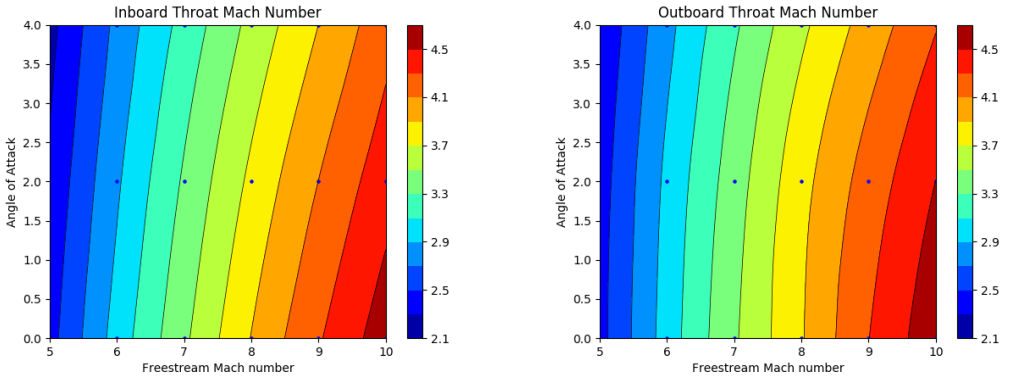

(a) **(b)**

Fig 8. Throat values for Mach number of the inboard and outboard engines

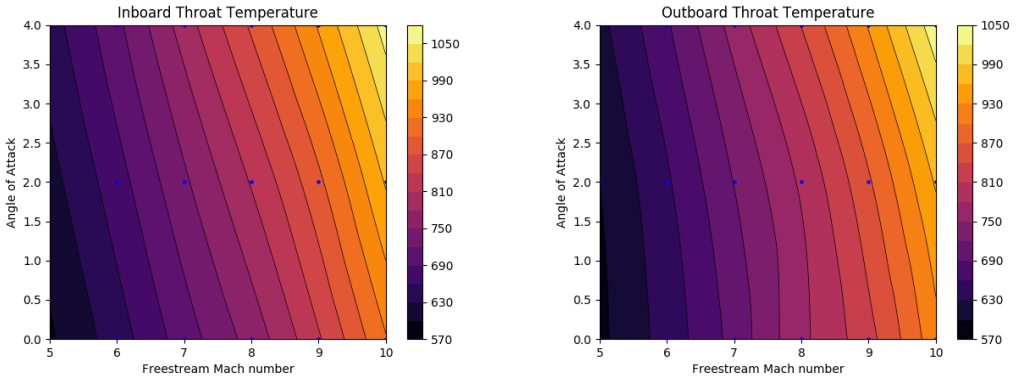

(a) **(b)**

Fig 9. Throat values for temperature of the inboard and outboard engines

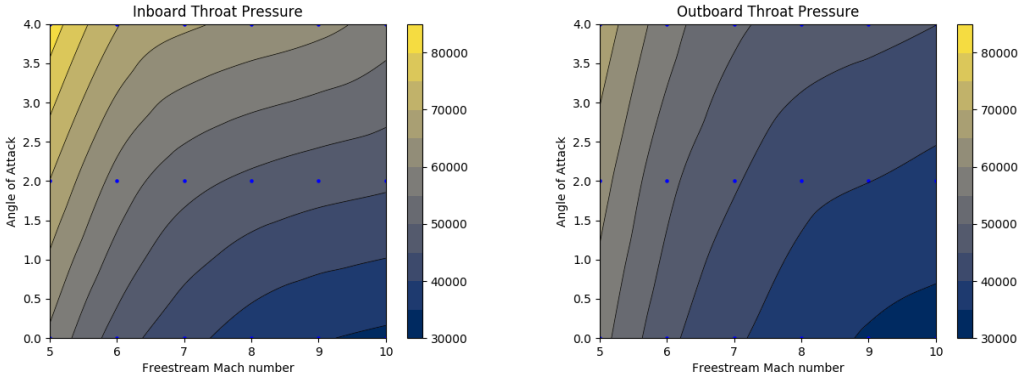

(a) **(b)**

Fig 10. Throat values for pressure of the inboard and outboard engines.

of the losses of the compression process. As expected, the pressure recovery decreases with increasing Mach number.

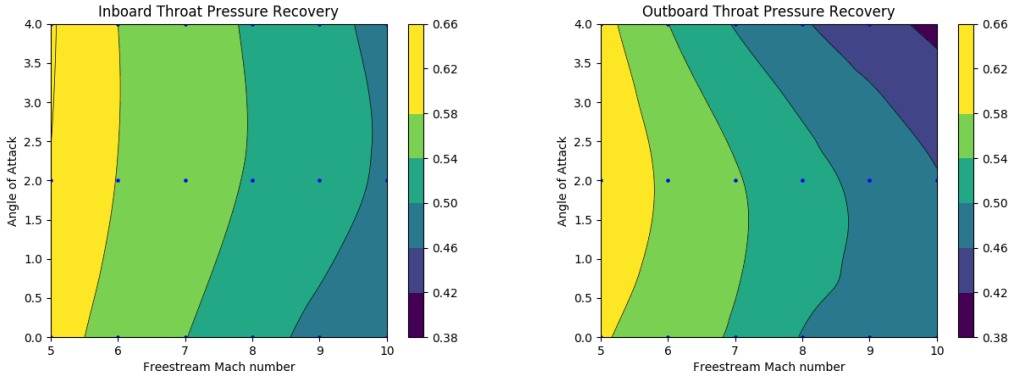

Fig 11. Throat values for pressure recovery of the inboard and outboard engines.

Figure 12 compares the mass flow rate ingested by the all inlets compared the their projected freestream area. This metric examines how much of the air potentially available to the engines is captured - some air is processed through the bow shock but not captured by the inlets, and it is important to understand what level this is to judge inlet performance. The inlets perform well when the bowshock sits closest to the vehicle i.e. at high Mach numbers and greater angles of attack. The steeper shock angles at low Mach numbers spill greater air, however lower performance at the lower Mach numbers is acceptable and indeed expected for a fixed geometry accelerator engine.

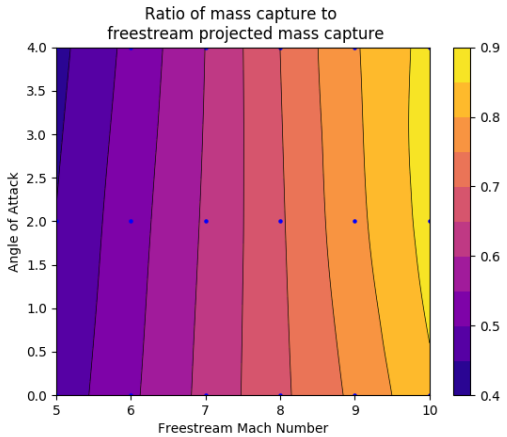

Fig 12. Ratio of captured to freestream projected mass flow rate.

The final inlet performance metric examined here is the kinetic energy efficiency, shown in Figure 13 with the efficiency evaluated for all inlet angles of attack and flight speed. Kinetic energy efficiency compares the kinetic energy achieved by the throat flow if it was isentropically expanded to the freestream pressure, to the freestream kinetic energy. This term is another way exploring the losses of the inlet. For comparison, Smart's correlation [9] is also shown in the diagram. The performance of the inlet is high, exceeding the empirical correlation of Smart. The general trend is also shown that the ratio between throat and freestream Mach number reduces with increasing freestream speed.

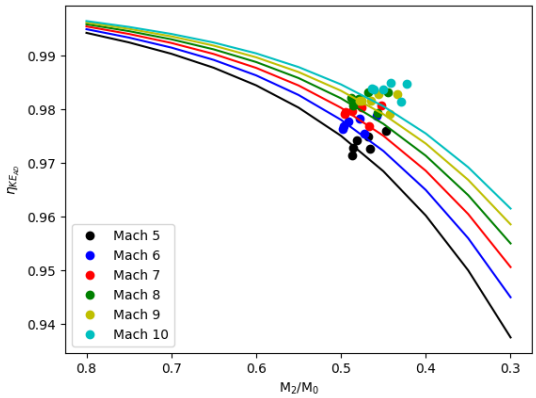

Fig 13. Kinetic energy efficiency of the inlets. The lines represent Smart's correlation for kinetic energy efficiency [9].

6. Conclusions

The CREST inlet was developed by Gollan and Smart to sit as a group of four underneath a conical, accelerating vehicle. The four inlet/engine modules were chosen as a balance of wetted area, penetration of fuel jets, and inlet shape transitioning behaviour. Importantly, the inlet has shown no separation from the cowl shock impinging on the bodyside boundary layer, which is a major benefit of this style of inlet.

This work has shown the CREST inlet to perform extremely well over the entire SPARTAN trajectory. Chiefly, it provides the combustion system with usable pressures and temperatures, and is able to do this with a high kinetic energy efficiency, and reasonable pressure recovery. At the start of the trajectory, forced ignition is likely required for all engines. The main difference between the inboard and outboard inlets is the mass capture variation, which leads to a reduced pressure for the outboard inlets. The temperature and Mach numbers remain consistent between the inlets throughout the trajectory. Reduced mass flow through the outboard inlets translates directly to lower thrust, and to slower combustion. This needs to be considered further in context of the inlet design.

The streamthrust averaged properties, while instructive in considering the overall inlet performance envelope, do not tell the complete story of the difference between the two inlets. Airframe integrated, streamline-traced scramjet engines have been shown to provide nonuniform inflow to the combustor. This is due to large variations in boundary layer thickness around the engine perimeter and interactions with the complex inlet geometry. How such an inlet performs with a skewed inflow has been answered here. Due to the lateral inflow of a cone at angle of attack, the outer half of each inlet interacts greater than the inside, developing some asymmetry between the geometric inlet halves. This asymmetry is higher for the outboard inlet.

The thickened (and laterally squished) bodyside boundary layer is swept towards the inner part of the inlet in both cases. This is usually targeted with inlet injection, and so further consideration is required when fuelling this. On the sidewalls, the inner spreading of the boundary layer is compressed longitudinally, closer to the bodyside boundary layer, and higher in temperature compared to the outer wall.

None of the asymmetric features pose any additional challenge to an engine designer over a standard stream-traced, airframe integrated engine design. The inlet performs extremely well in this regard.

Potentially the inlet design may be tweaked for performance on an angle of attack vehicle. The outboard inlet could be larger, to regain some mass capture on the inboard inlet. The outer leading edge of each

inlet may reach forward towards the tip of the conical forebody to sit better underneath the bow shock and compensate for the laterally moving inflow. This type of modification would make the inlets better suited to their off-centre location on the conical vehicle. However, altering the inlet shape in this way requires the entire vehicle and its performance over the trajectory to be considered at once, which would be prohibitively expensive.

7. Acknowledgements

This research was undertaken with the assistance of resources provided at the NCI National Facility and the Pawsey Supercomputing Centre through the National Computational Merit Allocation Scheme supported by the Australian Government.

References

[1] W. H. Heiser and D. T. Pratt, *Hypersonic airbreathing propulsion*. Aiaa, 1994.

[2] A. D. Ward and M. K. Smart, "Parametric study of the aftbody design of an airbreathing hypersonic accelerator," *Journal of Spacecraft and Rockets*, pp. 1–13, 2021.

[3] K. A. Damm, "Adjoint-based aerodynamic design optimisation in hypersonic flow," 2020.

[4] J. R. Henry and G. Y. Anderson, "Design considerations for the airframe-integrated scramjet," in *Intern. Symp. on Air Breathing Engines*, 1973.

[5] C. Edwards, W. Small, J. Weidner, and P. Johnston, "Studies of scramjet/airframe integration techniques for hypersonic aircraft," in *13th Aerospace Sciences Meeting*, 1975, p. 58.

[6] J. V. Becker and F. S. Kirkham, "Hypersonic transports," *Vehicle Technology for Civil Aviation-The Seventies and Beyond, NASA SP-292*, pp. 429–445, 1971.

[7] C. A. Trexler, "Performance of an inlet for an integrated scramjet concept," *Journal of Aircraft*, vol. 11, no. 9, pp. 589–591, 1974.

[8] R. H. Korkegi, "Comparison of shock-induced two-and three-dimensional incipient turbulent seperation," *AIAA journal*, vol. 13, no. 4, pp. 534–535, 1975.

[9] M. K. Smart, "How much compression should a scramjet inlet do?" *AIAA journal*, vol. 50, no. 3, pp. 610–619, 2012.

[10] A. Kumar and C. A. Trexler, "Analysis and performance prediction of scramjet inlets utilizing a three-dimensional navier-stokes code," 1986.

[11] M. Krause, B. Reinartz, and J. Ballmann, "Numerical computayions for designing a scramjet intake," in *25th International Congress of The Aeronautical Sciences*. Citeseer, 2006, pp. 3–8.

[12] W. Hartill, "Analytical and experimental investigation of a scramjet inlet of quadriform shape," *US Air Force, TR AFAPL-TR-65-74, Marquardt Corp*, 1965.

[13] M. Smart, "Design of three-dimensional hypersonic inlets with rectangular-to-elliptical shape transition," *Journal of Propulsion and Power*, vol. 15, no. 3, pp. 408–416, 1999.

[14] S. Pinckney, "Rectangular capture area to circular combustor scramjet engine," 1978.

[15] T. Taylor and D. VanWie, "Performance analysis of hypersonic shape-changing inlets derived from morphing streamline traced flowpaths," in *15th AIAA international space planes and hypersonic systems and technologies conference*, 2008, p. 2635.

[16] F. Xing, Y. Huang, C. Ruan, X. Fang, and Y. Yao, "Numerical investigation on two streamline-traced busemann inlet-isolators," in *54th AIAA Aerospace Sciences Meeting*, 2016, p. 0529.

[17] A. Borovikov, V. Gavriliouk, I. Gilevich, V. Duganov, A. Khokhlov, and V. Stepanov, "Gasdynamic design of supersonic and hypersonic airframe integrated inlets and nozzles," in *Space Plane and Hypersonic Systems and Technology Conference*, 1996, p. 4549.

[18] M. K. Smart and C. A. Trexler, "Mach 4 performance of hypersonic inlet with rectangular-to-elliptical shape transition," *Journal of Propulsion and Power*, vol. 20, no. 2, pp. 288–293, 2004.

[19] W. O. Landsberg, V. Wheatley, M. K. Smart, and A. Veeraragavan, "Enhanced supersonic combustion targeting combustor length reduction in a mach 12 scramjet," *AIAA Journal*, vol. 56, no. 10, pp. 3802–3807, 2018.

[20] J. E. Barth, V. Wheatley, and M. K. Smart, "Effects of hydrogen fuel injection in a mach 12 scramjet inlet," *AIAA Journal*, vol. 53, no. 10, pp. 2907–2919, 2015.

[21] M. Smart and E. Ruf, "Free-jet testing of a rest scramjet at off-design conditions," in *25th AIAA aerodynamic Measurement technology and ground testing Conference*, 2006, p. 2955.

[22] R. J. Gollan and M. K. Smart, "Design of modular shape-transition inlets for a conical hypersonic vehicle," *Journal of Propulsion and Power*, vol. 29, no. 4, pp. 832–838, 2013.

[23] T. Jazra, D. Preller, and M. Smart, "Design of an airbreathing second stage for a rocket-scramjet-rocket launch vehicle," *Journal of Spacecraft and Rockets*, vol. 50, no. 2, pp. 411–422, 2013.

[24] D. Preller and M. K. Smart, "Reusable launch of small satellites using scramjets," *Journal of Spacecraft and Rockets*, vol. 54, no. 6, pp. 1317–1329, 2017.

[25] M. Tetlow and C. Doolan, "Comparison of hydrogen and hydrocarbon-fueled scramjet engines for orbital insertion," *Journal of Spacecraft and Rockets*, vol. 44, no. 2, pp. 365–373, 2007.

[26] M. K. Smart and M. R. Tetlow, "Orbital delivery of small payloads using hypersonic airbreathing propulsion," *Journal of Spacecraft and Rockets*, vol. 46, no. 1, pp. 117–125, 2009.

[27] A. Kantrowitz *et al.*, "Preliminary investigation of supersonic diffusers," NATIONAL AERONAUTICS AND SPACE ADMIN LANGLEY RESEARCH CENTER HAMPTON VA, Tech. Rep., 1945.

[28] I. Nompelis, T. W. Drayna, and G. V. Candler, "Development of a hybrid unstructured implicit solver for the simulation of reacting flows over complex geometries," *AIAA Paper*, vol. 2227, p. 2004, 2004.

[29] J. E. Barth, "Mixing and combustion enhancement in a mach 12 shape-transitioning scramjet engine," Ph.D. dissertation, School of Mechanical and Mining Engineering, The Univ. of Queensland, Brisbane, Queensland, Australia, 2014.

[30] W. O. Landsberg, N. N. Gibbons, V. Wheatley, M. K. Smart, and A. Veeraragavan, "Improving scramjet performance through flow field manipulation," *Journal of Propulsion and Power*, pp. 1–13, 2017.

[31] D. Curran, V. Wheatley, and M. Smart, "Investigation of combustion mode control in a mach 8 shape-transitioning scramjet," *AIAA Journal*, pp. 2977–2988, 2019.

[32] R. W. MacCormack and G. V. Candler, "The solution of the navier-stokes equations using gauss-seidel line relaxation," *Computers & fluids*, vol. 17, no. 1, pp. 135–150, 1989.

[33] M. J. Wright, G. V. Candler, and D. Bose, "Data-parallel line relaxation method for the navier-stokes equations," *AIAA Journal*, vol. 36, no. 9, pp. 1603–1609, 1998.

[34] P. R. Spalart, S. R. Allmaras *et al.*, "A one equation turbulence model for aerodynamic flows," *RECHERCHE AEROSPATIALE-FRENCH EDITION-*, pp. 5–5, 1994.

[35] S. Catris and B. Aupoix, "Density corrections for turbulence models," *Aerospace Science and Technology*, vol. 4, no. 1, pp. 1–11, 2000.

[36] P. D. C. PDC. (2016) Gridpro software - automatic multiblock grid gen- eration system. White Plains, NY. Version 6.5SP1. [Online]. Available: www.gridpro.com

[37] F. Stern, R. V. Wilson, H. W. Coleman, and E. G. Paterson, "Comprehensive approach to verification and validation of cfd simulations—part 1: methodology and procedures," *Journal of fluids engineering*, vol. 123, no. 4, pp. 793–802, 2001.

[38] J. Barth, "Mixing and combustion enhancement in a mach 12 shape-transitioning scramjet engine," Ph.D. dissertation, University of Queensland, 2014.